

# CN-CBF: Composite Neural Control Barrier Function for Safe Robot Navigation in Dynamic Environments

Bojan Derajic<sup>1,2</sup>, Sebastian Bernhard<sup>1</sup> and Wolfgang Hönig<sup>2</sup>

**Abstract**—Safe navigation of autonomous robots remains one of the core challenges in the field, especially in dynamic and uncertain environments. One of the prevalent approaches is safety filtering based on control barrier functions (CBFs), which are easy to deploy but difficult to design. Motivated by the shortcomings of existing learning- and model-based methods, we propose a simple yet effective neural CBF design method for safe robot navigation in dynamic environments. We employ the idea of a composite CBF, where multiple neural CBFs are combined into a single CBF. The individual CBFs are trained via the Hamilton-Jacobi reachability framework to approximate the optimal safe set for single moving obstacles. Additionally, we use the residual neural architecture, which guarantees that the estimated safe set does not intersect with the corresponding failure set. The method is extensively evaluated in simulation experiments for a ground robot and a quadrotor, comparing it against several baseline methods. The results show improved success rates of up to 18% compared to the best baseline, without increasing the conservativeness of the motion. Also, the method is demonstrated in hardware experiments for both types of robots.

## I. INTRODUCTION

Motion planning and control of mobile robots in dynamic and unknown environments has been an active research field for decades and many advanced methods have been published. Safety filtering is one of the most prominent and well-established approaches to safety-critical scenarios. This approach functions by monitoring the nominal control and modifying it when necessary to preserve safe operation of the system. The nominal control is usually modified by a switching mechanism or through an optimization procedure [1]. In this paper, we follow the second approach, where we specifically utilize control barrier functions (CBFs).

CBFs are scalar functions defined on the system’s state space characterizing safe control invariant sets based on Nagumo’s Theorem on set invariance [2], [3]. In practice, the main advantage of using CBFs is highlighted for control-affine systems, where the safety filtering is reduced to solving a quadratic program (QP) and can be executed at a high rate [4]. Nevertheless, the main problem is in designing a proper CBF, and finding computationally tractable and data-efficient methods are an ongoing challenge [1]. Also, an additional layer of complexity is present for systems such as mobile robots that operate in dynamic and uncertain environments based on local perception. In such cases, the CBF must be generated in real time from the available

information, rendering the existing methods for offline CBF design ineffective [5].

In this paper, we propose a new approach to designing a CBF for mobile robots operating in dynamic environments. The goal is to safely navigate the environment without colliding with any obstacle, corresponding to the robot’s state entering a *failure set*. We first design a neural CBF for a single robot-obstacle pair and then apply an aggregation function that outputs a single composite CBF for an arbitrary number of individual CBFs. To recover the optimal safe sets for individual obstacles, as a CBF we use a neural approximation of the value function obtained via Hamilton-Jacobi (HJ) reachability analysis. Importantly, we apply HJ reachability to the relative dynamics of the robot and the obstacle rather than the robot dynamics directly, which results in the failure set being stationary instead of time-varying. Moreover, by using a residual neural architecture, we ensure that the estimated safe set of individual CBFs, as well as the composite CBF, never intersects the corresponding set of failure states. In summary, our contributions are:

- A neural CBF design method for dynamic environments that simultaneously recovers near-optimal safe sets for individual obstacles, guarantees the estimated safe set never intersects the failure set, and scales to an arbitrary number of obstacles — none of which is achieved jointly by existing approaches.
- Extensive evaluation of the proposed method against several relevant baselines in simulation experiments and hardware demonstration for two types of robots - a ground robot and a quadrotor.

## II. RELATED WORK

When it comes to safety-critical mobile robot deployment, two types of methods are prevalent: receding horizon approaches and safety filtering [6]. The first category comprises different MPC-based local planners (e.g., [7], [8], [9]), while the second is dominated by CBF-based methods [1], which we discuss further.

There is a significant amount of literature on CBF-based methods as they have been proven to be a powerful, yet elegant way to enforce safety [3]. Still, designing a proper CBF for a general nonlinear system with state and control constraints remains the major challenge [1]. The particularly relevant research leverages learning techniques to design CBFs in a more flexible way [10]. For example, learning CBFs from expert trajectories is proposed in [11], while the neural CBFs for systems with input limits are introduced

<sup>1</sup>AUMOVIO, Germany

<sup>2</sup>Technical University of Berlin, Germany

Contact e-mail: bojan.derajic@aumovio.com

This work is funded by the German Federal Ministry for Economic Affairs and Climate Action within the project *nextAIM*.

in [12]. Also, designing CBFs in real time via Gaussian splatting is used in [13]. However, these approaches often fail to recover the optimal safe set, which can be obtained via HJ reachability analysis [14].

The connection between CBFs and HJ reachability is established in [15], where the novel control-barrier value function (CBVF) is introduced as a method for the CBF design, but demonstrated only for known environments. Overcoming this disadvantage, the CBFs in [16] and [5] are observation-conditioned neural methods grounded in HJ reachability theory and approximately recover the maximal safe set. The first one uses residual architecture to ensure that the predicted safe set never intersects occupied space, while the second method includes uncertainty estimation. However, these methods do not consider dynamic obstacles explicitly. A neural approximation of a joint HJ value function for moving obstacles is used in [9], but is limited to a low number of obstacles due to combinatorial complexity. Instead, we apply HJ reachability to dynamic environments by aggregating multiple HJ functions into a single function, reducing the total time required for data generation and model training from dozens of hours to minutes.

The idea of composite CBFs has been explored in several previous works. The authors in [17] propose a composite CBF tailored for safe quadrotor navigation only in static environments. Time-varying safety constraints are considered in [18], but the safe control is provided in a closed form without imposing actuation limits. The method proposed in [19] learns interaction dynamics between the robot and an obstacle from data and uses a non-smooth aggregation function, resulting in complicated training process, suboptimal safe set, and non-smooth composite CBF. On the other hand, we introduce a smooth learning-based composite CBF approach that handles dynamic obstacles and respects the actuation limits of the robot.

### III. PRELIMINARIES

In this section, we present a brief overview of the two frameworks serving as the basis for our approach — CBFs and HJ reachability. We assume a continuous-time setting, but for readability, we omit the time variable  $t$  where it is not crucial.

#### A. Control Barrier Functions

We consider control-affine system dynamics

$$\dot{x} = f(x) + g(x)u \quad (1)$$

where  $x \in \mathcal{X} \subset \mathbb{R}^{n_x}$  and  $u \in \mathcal{U} \subset \mathbb{R}^{n_u}$ . A continuously differentiable function  $h : \mathcal{X} \times [0, \infty) \rightarrow \mathbb{R}$  is a valid control barrier function if there exists an extended class  $\kappa$  function  $\alpha : \mathbb{R} \rightarrow \mathbb{R}$  such that

$$\sup_{u \in \mathcal{U}} \nabla_x h(x, t)^\top \dot{x} + \frac{\partial h(x, t)}{\partial t} \geq -\alpha(h(x, t)). \quad (2)$$

If we define set  $\mathcal{S}$  as

$$\mathcal{S}(t) = \{x \in \mathcal{X} : h(x, t) > 0\}, \quad (3)$$

then  $\mathcal{S}(t)$  is forward invariant and we call it *safe set* [20].

When the admissible control set  $\mathcal{U}$  can be expressed through linear constraints, the CBF condition (2) can be leveraged to construct a QP-based safety filter [4]. Given the current state  $x$  and a nominal (reference) input  $u_{ref}$ , the CBF-QP provides a safe control  $u^*$  by solving the following optimization problem:

$$\begin{aligned} u^* &= \arg \min_{u \in \mathcal{U}} \frac{1}{2} \|u_{ref} - u\|^2 \\ s.t. \quad &L_f h(x, t) + L_g h(x, t)u + \frac{\partial h(x, t)}{\partial t} + \alpha(h(x, t)) \geq 0, \end{aligned} \quad (4)$$

where  $L_f h(x, t)$  and  $L_g h(x, t)$  are the Lie derivatives with respect to  $f(x)$  and  $g(x)$ , respectively.

#### B. Hamilton-Jacobi Reachability Analysis

HJ reachability is a framework for verification and analysis of dynamical systems based on the optimal control theory [21]. In general, here we consider a general system dynamics

$$\dot{x} = f(x, u, d), \quad (5)$$

where  $u \in \mathcal{U} \subset \mathbb{R}^{n_u}$  and  $d \in \mathcal{D} \subset \mathbb{R}^{n_d}$  are two competing inputs. If the system starts at state  $x(t)$ , then  $\xi_{x,t}^{u,d}(\tau)$  is the system's state at time  $\tau$  after applying  $u(\cdot)$  and  $d(\cdot)$  over time horizon  $[t, \tau]$ . The set of states that should be ultimately avoided is called a failure set  $\mathcal{F}$ . Also, we define a backward reachable tube (BRT)  $\mathcal{B}(t)$ , which is a set of initial states for which exists  $d(\cdot)$  such that the system will reach  $\mathcal{F}$  within the time horizon  $[t, T]$  for any control  $u(\cdot)$ , i.e.

$$\mathcal{B}(t) = \{x : \exists d(\cdot), \forall u(\cdot), \exists \tau \in [t, T], \xi_{x,t}^{u,d}(\tau) \in \mathcal{F}\}. \quad (6)$$

To compute the BRT for a given  $\mathcal{F}$ , we define it as the zero-sublevel set of a failure function  $\ell(x)$ , i.e.  $\mathcal{F} = \{x : \ell(x) \leq 0\}$ . The computation of the BRT can be formulated as a min-max optimization problem where the objective is the minimal distance to  $\mathcal{F}$  over the time horizon:

$$J(x, u(\cdot), d(\cdot), t) = \min_{\tau \in [t, T]} \ell(\xi_{x,t}^{u,d}(\tau)). \quad (7)$$

The control input  $u$  keeps the system trajectory away from the failure region  $\mathcal{F}$ , while the adversarial input  $d$  pushes it toward  $\mathcal{F}$ . This can be described by the value function

$$V(x, t) = \inf_{d(\cdot) \in \mathcal{D}} \sup_{u(\cdot) \in \mathcal{U}} \{J(x, u(\cdot), d(\cdot), t)\}. \quad (8)$$

This value function can be computed using the dynamic programming principle to solve the following Hamilton-Jacobi-Isaacs Variational Inequality [21]:

$$\begin{aligned} \min \left\{ \frac{\partial}{\partial t} V(x, t) + H(x, t), \ell(x) - V(x, t) \right\} &= 0, \\ V(x, T) &= \ell(x). \end{aligned} \quad (9)$$

In the formulation above, Hamiltonian  $H(x, t)$  is defined as

$$H(x, t) = \max_{u \in \mathcal{U}} \min_{d \in \mathcal{D}} \nabla V(x, t)^\top f(x, u, d). \quad (10)$$

Once the value function (8) is obtained, the corresponding BRT is zero-sublevel set of  $V(x, t)$ , i.e.

$$\mathcal{B}(t) = \{x : V(x, t) \leq 0\}, \quad (11)$$

and the maximal safe set is its complement:  $\mathcal{S}(t) = \mathcal{B}(t)^c$ .

Assuming terminal time  $T = 0$  and static  $\ell(x)$ , we propagate the value function backward in time until it converges to its steady-state value  $V(x) = \lim_{t \rightarrow -\infty} V(x, t)$  and then use  $V(x)$  as the target CBF during training.

#### IV. METHODOLOGY

In this section, we present a detailed description of the proposed CN-CBF method. We first clarify the assumed structure of the problem, and then proceed with further explanation. Our focus is on dynamic environments where safety constraints evolve over time. This condition is explicitly taken into account in (2) as a partial time derivative of the CBF, representing a change of the safe set due to the motion of obstacles. We first consider a scenario with a single moving obstacle, and later extend the method for an arbitrary number of obstacles.

Obtaining a CBF with the optimal safe set for the single obstacle case is possible via HJ reachability framework [14], [1]. A direct approach would be to define a time-dependent failure function  $\ell(x, t)$  based on the motion of the obstacle, which is generally impractical. Instead, we consider a moving obstacle as a dynamical system with a state vector  $o \in \mathcal{O} \subset \mathbb{R}^{n_o}$  whose dynamics evolve according to

$$\dot{o} = \nu(o, d), \quad (12)$$

where  $d \in \mathcal{D} \subset \mathbb{R}^{n_d}$  is the input to the system. Next, since only the relative motion of the robot and the obstacle matters, we define a transformation  $\rho : \mathbb{R}^{n_x} \times \mathbb{R}^{n_o} \rightarrow \mathbb{R}^{n_z}$  which outputs a relative state vector  $z \in \mathcal{Z} \subset \mathbb{R}^{n_z}$ , i.e.

$$z = \rho(x, o). \quad (13)$$

The relative dynamics is then obtained as

$$\begin{aligned} \dot{z} &= \frac{\partial z}{\partial x} \dot{x} + \frac{\partial z}{\partial o} \dot{o} \\ &= \zeta(z, u, d). \end{aligned} \quad (14)$$

The transformation  $\rho$ , i.e. relative state  $z$ , is a design choice and depends on the concrete robot and (assumed) obstacle dynamics. Typically, the relative state contains relative pose and velocity. In Section V we provide concrete examples for a ground robot and a quadrotor navigating in a crowd.

The advantage of using a relative state representation in such a setting is twofold. First, the failure function  $\ell(z)$  defined for the relative state is stationary because a fixed set of relative states is considered a failure regardless of the absolute motion of the robot and the obstacle. Second, the relative dynamics (14) has two competing inputs — the robot's input  $u$  driving the relative state from the failure region, and the obstacles input  $d$  driving it toward the failure region. This makes (14) exactly the type of system considered in the HJ reachability framework, allowing the application of existing tools.

Motivated by the discussion above, we design a CBF for the relative dynamics rather than the original robot dynamics (1). Our aim is to use the value function obtained by HJ reachability as a relative CBF with the maximal safe set. However, numerical tools for HJ reachability provide only the numerical values of the value function on the predefined state-space grid. This means that the deployed CBF would require considerable memory to store these values and an additional interpolation logic to obtain the value and gradient for a given state. Instead, we use a neural approximation of the value function, allowing for lower memory requirements and efficient value and gradient queries via automatic differentiation.

Besides, we recall that the HJ value function defined in (8) is less than or equal to the failure function, so for relative dynamics we have  $V(z, t) \leq \ell(z)$ ,  $\forall z \in \mathcal{Z}$ ,  $\forall t$  [9], [16]. Therefore, assuming that the value function converged in time, we can write  $V(z) = \ell(z) - r(z)$  where  $r(z) \geq 0$ ,  $\forall z \in \mathcal{Z}$  is the residual function. Since  $\ell(z)$  is usually defined as a signed distance function that can be obtained efficiently in real time, we can approximate only the residual component. By defining the relative CBF as  $\bar{h}(z) := V(z)$  and approximating the residual function with a neural model with parameters  $\Theta$ , we have

$$\bar{h}_\Theta(z) = \ell(z) - r_\Theta(z). \quad (15)$$

Moreover, if the neural model has a non-negative activation function at the output, i.e.  $r_\Theta(z) \geq 0$ ,  $\forall z \in \mathcal{Z}$ , it is guaranteed that the learned safe set of  $\bar{h}_\Theta(z)$  never intersects the failure set defined by  $\ell(z)$  [16].

Nevertheless, to make the learned CBF usable, it is necessary to establish a relation between  $\bar{h}_\Theta(z)$  and the initial CBF constraint defined for robot dynamics (2). If we consider relative dynamics (14), we have

$$h(x, t) = \bar{h}_\Theta(z) \quad (16a)$$

$$\nabla_x h(x, t)^\top = \nabla_z \bar{h}_\Theta(z)^\top \frac{\partial z}{\partial x} \quad (16b)$$

$$\frac{\partial h(x, t)}{\partial t} = \nabla_z \bar{h}_\Theta(z)^\top \frac{\partial z}{\partial o} \dot{o} \quad (16c)$$

which completely defines the constraint in (2) and enables safe control. From the equations above, it is evident that the partial time derivative of the CBF is nonzero solely due to obstacle dynamics, which aligns with our expectations.

The next step is to extend the proposed method for multiple obstacles. To do so, we use the idea of the composite CBF where multiple CBFs are designed (typically one per obstacle) and combined into a single CBF using some aggregation function [22], [17]. Therefore, if there are  $M$  obstacles with states  $\{o_i\}_{i=1}^M$ , for the given robot state  $x$  we first obtain the set of relative states  $\{z_i\}_{i=1}^M$  and compute the corresponding relative CBFs  $\{\bar{h}_\Theta(z_i)\}_{i=1}^M$ . Then, we simply apply the aggregation function  $\eta : \mathbb{R}^M \rightarrow \mathbb{R}$  to obtain a single CBF value, i.e.

$$h_\Theta(z_1, \dots, z_M) = \eta(\bar{h}_\Theta(z_1), \dots, \bar{h}_\Theta(z_M)). \quad (17)$$

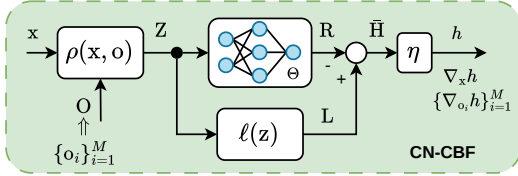


Fig. 1. CN-CBF structure.

In this paper, as the aggregation function, we use smooth under-approximation of the min function [20] defined as:

$$\eta(\bar{h}_{\Theta}(z_1), \dots, \bar{h}_{\Theta}(z_M)) = -\frac{1}{\beta} \ln \sum_{i=1}^M e^{-\beta \bar{h}_{\Theta}(z_i)}, \quad (18)$$

where  $\beta \in \mathbb{R}_+$  is the smoothing parameter. This particular choice of  $\eta$  ensures that the composite BRT is a superset of the union of individual BRTs and that the composite CBF is differentiable [22].

Similarly to the single-obstacle case, we can establish a relation between the composite CBF and the CBF constraint in (2) as:

$$h(x, t) = h_{\Theta}(\{z\}_{i=1}^M) \quad (19a)$$

$$\nabla_x h(x, t)^{\top} = \sum_{i=1}^M \nabla_{z_i} h_{\Theta}(\{z\}_{i=1}^M)^{\top} \frac{\partial z_i}{\partial x} \quad (19b)$$

$$\frac{\partial h(x, t)}{\partial t} = \sum_{i=1}^M \nabla_{z_i} h_{\Theta}(\{z\}_{i=1}^M)^{\top} \frac{\partial z_i}{\partial o_i} \dot{o}_i \quad (19c)$$

An important practical note is that if all the functions are implemented using a framework that supports automatic differentiation (e.g., PyTorch), the CBF value and its gradients can be obtained in a single forward and backward pass. This is important since the derivation of the analytical expressions for gradients might be overly complex. First, the set of obstacle states  $\{o_i\}_{i=1}^M$  is converted in a tensor (batch of vectors)  $O \in \mathbb{R}^{M \times n_o}$ . For the current robot state  $x$  and based on  $O$ , we form a tensor of relative states  $Z \in \mathbb{R}^{M \times n_z}$  which is propagated through the neural model to obtain tensor of residuals values  $R \in \mathbb{R}^M$ , while in parallel a tensor of failure function values  $L \in \mathbb{R}^M$  is computed. Then, by subtracting  $R$  from  $L$  we get  $\bar{H}$  and finally by applying  $\eta$  the composite CBF value is computed. We call this method composite neural CBF (CN-CBF) and the described procedure is visualized in Fig. 1.

It should be noted that the number of obstacles  $M$  is not predefined and can change over time, making the approach particularly flexible and scalable. However, whenever the number  $M$  changes, there is a discontinuity in the composite CBF that might affect the behavior of the safety filter. From the aspect of safety, we are interested in the case when  $M$  increases, as it enlarges the unsafe region and states that were safe suddenly become unsafe. Therefore, to ensure continual safety, it is required that the newly observed obstacles do not render the current robot's state unsafe instantly [16]. In practice, this can be ensured to some extent by using a sensor with a sufficiently large perception field.

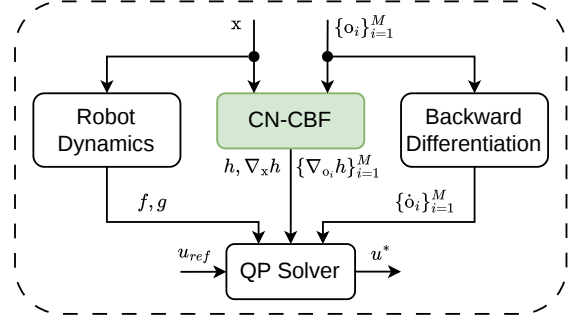


Fig. 2. Block diagram of the proposed CN-CBF safety filter.

The final stage of the proposed approach is to integrate the CN-CBF into a CBF-QP safety filter defined in (4). The CN-CBF model provides the CBF value and gradients with respect to the robot and obstacle states. However, the CBF constraint formulation (2) also requires  $f(x), g(x)$  and  $\{\dot{o}_i\}_{i=1}^M$ , which we can compute in parallel to the CN-CBF block. The time derivative of the  $i$ th obstacle state at time  $t$  is approximated using the backward differentiation scheme<sup>1</sup>:

$$\dot{o}_i(t) \approx \frac{o_i(t) - o_i(t - \delta t)}{\delta t}, \quad (20)$$

where  $\delta t$  is the time period between the two successive observations. The overall architecture of the safety filter is presented in Fig. 2.

## V. EXPERIMENTAL RESULTS

We evaluate the proposed method in simulation experiments<sup>2</sup> for two types of mobile robots - a ground robot and a quadrotor. In the following subsection, we provide details on the implementation of the experiments.

### A. Simulation Experiments

The proposed CN-CBF safety filter and the baseline methods are evaluated in the Gazebo simulator. The testing environment consists of pedestrians walking within a rectangular space between random goal positions in a cyclic fashion. The agents are controlled by HuNavSim [23], which implements the social force model (SFM). Besides, the agents do not try to avoid the robot, meaning that collision avoidance must be ensured by the robot.

**Ground robot** is the first robot type that we analyze in our experiments. This robot is modeled as a kinematic unicycle with state vector  $x = [x_r, y_r, \theta_r]^{\top}$ , where  $x_r$  and  $y_r$  are positional coordinates and  $\theta_r$  is the heading angle. The control vector includes the linear speed  $v_r$  and the angular speed  $\omega_r$ , i.e.  $u = [v_r, \omega_r]^{\top}$ , while the dynamics equation is

$$\dot{x} = [v_r \cos(\theta_r) \quad v_r \sin(\theta_r) \quad \omega_r]^{\top} \quad (21)$$

with control limits  $v_r = [0.25, 1.0]$  and  $\omega_r \in [-0.8, 0.8]$ .

<sup>1</sup>If the perception module provides  $\dot{o}_i(t)$  directly, this block can be excluded from the safety filter. Also, more advanced estimation methods can be used in the presence of high noise.

<sup>2</sup>The code will be released upon publication of the paper.

The motion of a pedestrian (i.e., an obstacle) is described by the unicycle model with a state vector  $o = [x_o, y_o, \theta_o, v_o]^\top$  and input vector  $d = \omega_o$ , where  $\omega_o \in [-0.35, 0.35]$ . This choice is motivated by the observation that pedestrians in open spaces most of the time walk toward their goal positions with roughly constant speed and a certain change in orientation necessary to avoid other people. This model can be seen as a more robust constant velocity (CV) model that allows for a change in motion direction. Regarding state and input limits, one can collect a dataset of pedestrian motion in a crowd and compute distributions of speed, turning rate, etc. Then, the state and input limits in the HJ reachability can be chosen to cover the major part of those distributions, achieving a trade-off between robustness and conservativeness.

We define  $z = [x_{rel}, y_{rel}, \theta_{rel}, v_o]^\top$  as relative state vector, where  $x_{rel}, y_{rel}$  is relative position and  $\theta_{rel}$  is relative angle expressed in the robot's frame of reference<sup>3</sup>, and  $v_o$  is the obstacle's speed. This choice of relative states results in the following relative dynamics:

$$\dot{z} = \begin{bmatrix} -v_r + v_o \cos \theta_{rel} + \omega_r y_{rel} \\ v_o \sin \theta_{rel} - \omega_r x_{rel} \\ \omega_o - \omega_r \\ 0 \end{bmatrix}. \quad (22)$$

A collision between the robot and an obstacle occurs when the relative distance is less than or equal to  $R_{min} = R_r + R_o$ , where  $R_r$  is the radius of the robot and  $R_o$  is the radius of the obstacle. Based on that, the failure function is defined as  $\ell(z) = \sqrt{x_{rel}^2 + y_{rel}^2} - R_{min}$ . The residual function  $r_\Theta(z)$  is approximated by a multi-layer perceptron (MLP) model with the following architecture: 4 input units, 6 hidden layers (48-48-24-24-12-12 units) with sin activations, and a single output with softplus activation. The training data is generated using the `hj_reachability`<sup>4</sup> Python package for a state-space grid of shape  $80 \times 80 \times 20 \times 10$ . The model is trained for 10 000 epochs using the Adam optimizer. The computation of the HJ value function takes  $\sim 10$  seconds, while the model training process takes  $\sim 5.5$  minutes on a single GTX 3090 GPU, making the proposed approach more computationally efficient compared to other learning-based approaches. For comparison, the method in [9] takes  $\sim 20$ h for data generation and  $\sim 15$ h for model training in the same setting. Also, the total number of model parameters is 4837, which is significantly lower than  $1.28 \times 10^6$  values that would be stored in case of a look-up approach. The positional slice of the neural CBF for relative dynamics is visualized in Fig. 3 for  $\theta_{rel} = \pi$  and  $v_o = 1.2$ . It can be seen that the zero-level set of the neural CBF does not intersect the failure region and accurately approximates the true zero-level set.

We compare our approach against several advanced MPC-based local planners with different representations of safety constraints that have been shown effective in practice: SDF-MPC [24], DCBF-MPC [25], VO-MPC [26] and RNTC-

<sup>3</sup>We could also express it in the world frame, but the relative dynamics  $\dot{z}$  could not be formulated as a function of  $z$  directly in this particular case.

<sup>4</sup>[https://github.com/StanfordASL/hj\\_reachability](https://github.com/StanfordASL/hj_reachability)

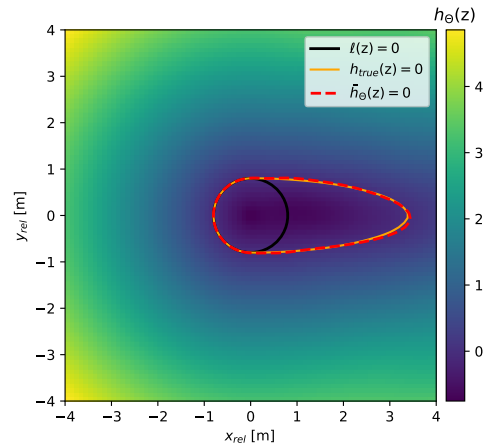


Fig. 3. Slice of the learned neural CBF for relative dynamics in the case of the ground robot ( $\theta_{rel} = \pi$ ;  $v_o = 1.2$ ).

MPC [9]. As the nominal controller for the proposed CN-CBF safety filter we use an MPC planner without a perception module, meaning that it drives the robot toward the reference state without any safety constraints. All MPC planners and the CBF safety filter are implemented using CasADi [27] and wrapped as ROS 2 nodes. For solving NLP problems in MPC planners we use the IPOPT solver, while for QP problems in the CBF filter we use qpOASES. The MPCs run at a control frequency of 20 Hz and a prediction horizon of 2 s (sampling time 0.1 s), while the safety filter runs at 250 Hz. As the  $\kappa$  function in (2) we use linear function  $\alpha(h(x)) = kh(x)$  with  $k = 4.0$ , while the smoothing parameter in (18) is set to  $\beta = 4.0$ . These parameters are simply tuned using a grid search approach.

For the experiments, we first generate 100 random scenarios for 5, 10 and 15 pedestrians, and then test all the methods for the same set of scenarios. The pedestrians are spawned at random locations and move between random goal positions within a rectangular area, thus keeping the effective obstacle density constant over time. The task is to navigate the robot from the start to the goal position without any collisions. As the main metric, we consider the success rate, i.e., the percentage of completed experiments without collision. Additionally, we report path length and time to reach the goal as additional indicators of motion quality.

The results are presented in Fig. 4. The proposed CN-CBF method clearly achieves higher success rates in all cases, with the performance gap widening significantly as obstacle density increases. Moreover, path length and time-to-goal are comparable to, or better than, the baselines. This is important because higher success rates can also result from overly conservative motion. In Fig. 5, we visualize one sample scenario from the ground robot simulation experiments.

The main reason why the success rate of the CN-CBF method decreases is that the error of the composite CBFs approximating the true joint HJ value function increases with increased obstacle density. Nevertheless, the performance is significantly better compared to the approaches that directly

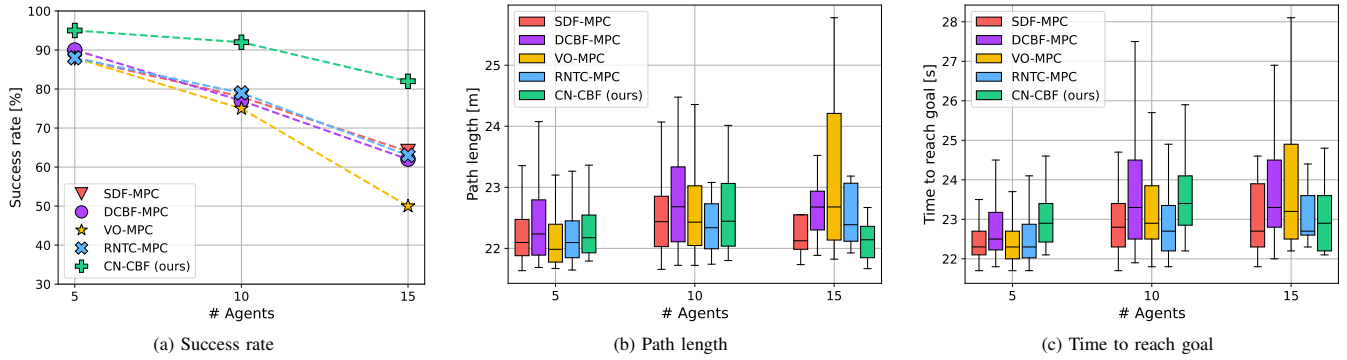


Fig. 4. Results from the simulation experiments with the ground robot model.

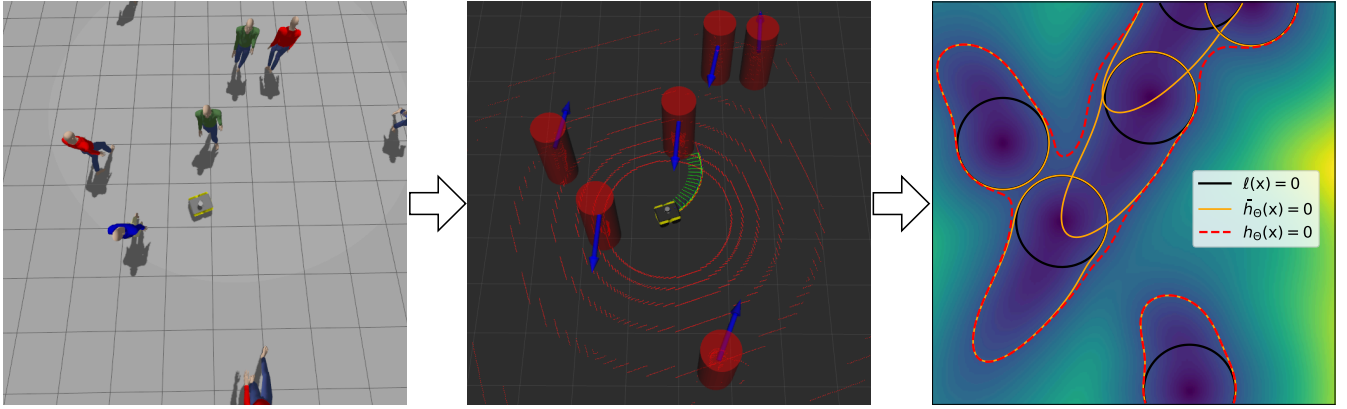


Fig. 5. An example scene from the simulation experiments with the ground robot model, which includes the 3D simulator (left), visualization of the local perception (middle), and the corresponding slice of the CN-CBF backprojected to the world frame (right).

approximate the joint value function, such as RNTC-MPC [9]. Other reasons for performance degradation include a limited sensing range and errors in the assumed obstacle dynamics, e.g., when pedestrians abruptly change direction in their motion.

**Quadrotor** is the second robot type we analyze in our experiments, which is modeled as a 2D double integrator with state vector  $x = [x_r, y_r, v_{x,r}, v_{y,r}]^\top$  and control vector  $u = [a_{x,r}, a_{y,r}]^\top$ . The dynamics of the robot is

$$\dot{x} = [v_{x,r} \quad v_{y,r} \quad a_{x,r} \quad a_{y,r}]^\top \quad (23)$$

where  $v_{x,r}, v_{y,r} \in [-2, 2]$  and  $a_{x,r}, a_{y,r} \in [-2, 2]$ .

In this case, the pedestrians are also modeled as 2D double integrators with state vector  $o = [x_o, y_o, v_{x,o}, v_{y,o}]^\top$  and input vector  $d = [a_{x,o}, a_{y,o}]^\top$  where  $v_{x,o}, v_{y,o} \in [-1.5, 1.5]$  and  $a_{x,o}, a_{y,o} \in [-1.0, 1.0]$ . This obstacle dynamics choice is essentially equivalent to the pedestrian model used in the ground robot case since  $v_{x,o} = v_o \cos(\theta_o)$  and  $v_{y,o} = v_o \sin(\theta_o)$ . However, here we can define the relative state simply as  $z = o - x$  with all states being expressed in the world frame, resulting in 2D double integrator relative dynamics:

$$\dot{z} = \begin{bmatrix} v_{x,o} - v_{x,r} \\ v_{y,o} - v_{y,r} \\ a_{x,o} - a_{x,r} \\ a_{y,o} - a_{y,r} \end{bmatrix}. \quad (24)$$

For the neural model of relative CBF, we use exactly the same MLP architecture and training hyperparameters as in the case of the ground robot. The training data is generated in the same way, but for a state-space grid of shape  $80 \times 80 \times 20 \times 20$ . Also, other implementation details and hyperparameters are the same as in the previous case.

As the baseline methods we use two other types of CBFs: collision cone CBF (C3BF) [28] and higher-order CBF (HO-CBF) [29] as they are particularly suited for this type of robot dynamics. The C3BF defines the safety constraint in the velocity space with the aim of preventing the relative velocity vector from entering the collision cone. The HO-CBF uses an SDF function as a CBF and enforces safety by constraining higher-order time derivative (in this case second-order). In both cases, the  $\kappa$  functions are linear functions with linear coefficients  $k = 3.0$  for C3BF and  $k_1 = 3.0, k_2 = 2.0$  for HO-CBF.

The nominal controller is an LQR, and as in the ground robot case, we generate 100 random scenarios for 5, 10, 15, and 20 pedestrians and test each method on the same set of scenarios. Again, the task is to navigate from the start to the goal position without any collision. The results from these experiments are presented in Fig. 6. Again, it can be seen that our method achieves the best performance, both in terms of success rates and motion efficiency.

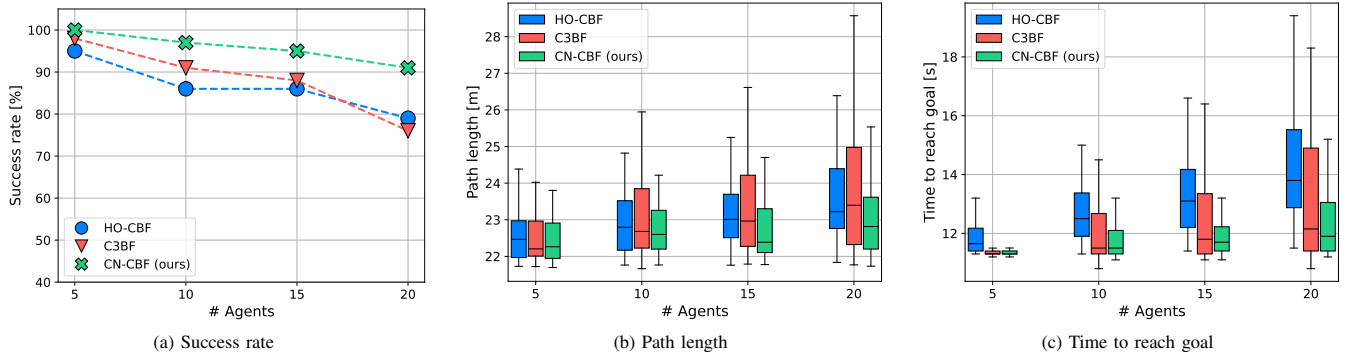


Fig. 6. Results from the simulation experiments with the quadrotor model.

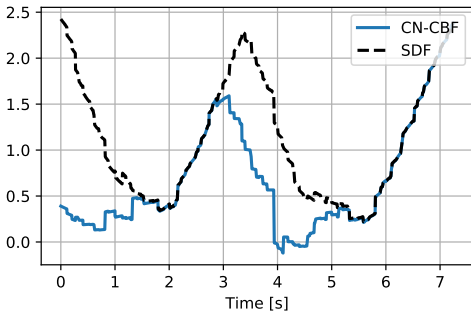


Fig. 7. CN-CBF and SDF values over time in the hardware experiments with the ground robot during successful collision avoidance.

### B. Hardware Experiments

The proposed CN-CBF method is deployed on a ground robot and a quadrotor in hardware experiments to demonstrate real-time feasibility and practical utility<sup>5</sup>. For the ground robot, we use a last-mile delivery robot equipped with 3D LiDAR, a stereo camera, and perception software for detecting moving objects. As in the simulations, the nominal controller is an MPC planner without safety constraints, and collision avoidance relies entirely on the safety filter. The robot and obstacle dynamics are also the same as in simulation, and all computation is performed onboard. In Fig. 7, we show the CN-CBF and SDF values over time during successful collision avoidance with pedestrians. The CBF value reaches small negative values due to model mismatch and noisy measurements, but no collision occurs due to a small buffer zone that compensates for these uncertainties.

We also conduct hardware experiments with a Crazyflie quadrotor where we compare our CN-CBF method against C3BF and HO-CBF in a collision avoidance task with five moving obstacles. The robot and obstacle dynamics, and the nominal controller are the same as in the simulation experiments. In this case obstacles are other drones moving between predefined waypoints. The results obtained are visualized in Fig. 8, showing the change over time for the CBF and SDF values. Only our method successfully prevents a collision, while the two baselines collide. Note

<sup>5</sup>For a visual demonstration, see the supplemental video.

that the baselines form a CBF per obstacle, while our method constructs only one composite neural CBF<sup>6</sup>.

## VI. LIMITATIONS AND FUTURE WORK

In this work, we obtain the true HJ value function using a numerical toolbox, which is limited to relatively low-dimensional systems due to the curse of dimensionality. To improve on this, one can use neural solvers like [30] or even combine it with MPC [31] to obtain an approximate solution. Also, we are assuming certain obstacle dynamics for the given environment. However, in some cases, it might not be possible to formulate a simple obstacle dynamics, and a more flexible approach would be necessary.

Regarding the future work, our aim is to extend the proposed method to heterogeneous environments with different types of obstacles, where neural CBFs defined for different relative dynamics would be combined into a single composite CBF. In addition, the goal is to improve flexibility and safety by replacing the aggregation function with a trainable model, thereby enabling a better approximation of the true joint CBF.

## VII. CONCLUSIONS

In this paper, we propose a novel CBF design method, called CN-CBF, suited for safe robot navigation in dynamic environments. The method is based on the idea of composite CBFs, where multiple neural CBFs are combined into a single CBF using an aggregation function. The individual CBFs approximate value function obtained by applying HJ reachability analysis to the relative dynamics between the robot and an obstacle. In this way, the relative CBFs approximately recover the maximal safe set, while the failure function used in HJ reachability remains stationary. Moreover, by using residual architecture for the individual CBFs, it is guaranteed that the estimated safe set never intersects with the observed failure set. The method is extensively evaluated in simulation experiments and demonstrated in the real world for two types of robots - a ground robot and a quadrotor. The results show improved performance in terms of safety without increasing motion conservativeness or computational complexity.

<sup>6</sup>The data after collision in the case of the baselines correspond to recovering behavior.

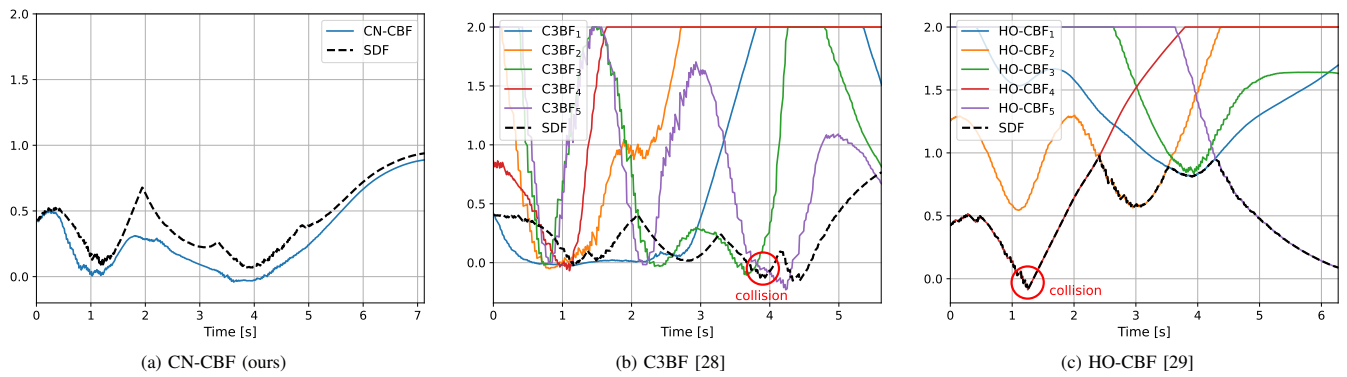


Fig. 8. CBF and SDF values for different methods obtained in hardware experiments with the quadrotor.

## REFERENCES

- [1] K.-C. Hsu, H. Hu, and J. F. Fisac, "The Safety Filter: A Unified View of Safety-Critical Control in Autonomous Systems," *Annual Review of Control, Robotics, and Autonomous Systems*, vol. 7, no. Volume 7, 2024, pp. 47–72, 2024.
- [2] M. Nagumo, "Über die Lage der Integralkurven gewöhnlicher Differentialgleichungen," *Proceedings of the Physico-Mathematical Society of Japan. 3rd Series*, vol. 24, pp. 551–559, 1942.
- [3] A. D. Ames, S. Coogan, M. Egerstedt, G. Notomista, K. Sreenath, and P. Tabuada, "Control Barrier Functions: Theory and Applications," in *European Control Conference (ECC)*, 2019, pp. 3420–3431.
- [4] A. D. Ames, J. W. Grizzle, and P. Tabuada, "Control barrier function based quadratic programs with application to adaptive cruise control," in *IEEE Conference on Decision and Control*, 2014, pp. 6271–6278.
- [5] A. Lin, S. Peng, and S. Bansal, "One Filter to Deploy Them All: Robust Safety for Quadrupedal Navigation in Unknown Environments," *IEEE Transactions on Robotics*, vol. 42, pp. 545–560, 2026.
- [6] S. Hwang, I. Jang, D. Kim, and H. J. Kim, "Safe Motion Planning and Control for Mobile Robots: A Survey," *International Journal of Control, Automation and Systems*, vol. 22, no. 10, pp. 2955–2969, 2024.
- [7] B. Brito, B. Floor, L. Ferranti, and J. Alonso-Mora, "Model Predictive Contouring Control for Collision Avoidance in Unstructured Dynamic Environments," *IEEE Robotics and Automation Letters*, vol. 4, no. 4, pp. 4459–4466, 2019.
- [8] S. Samavi, J. R. Han, F. Shkurti, and A. P. Schoellig, "SICNav: Safe and Interactive Crowd Navigation Using Model Predictive Control and Bilevel Optimization," *IEEE Transactions on Robotics*, vol. 41, pp. 801–818, 2025.
- [9] B. Derajic, M.-K. Bouzidi, S. Bernhard, and W. Hönig, "Residual Neural Terminal Constraint for MPC-based Collision Avoidance in Dynamic Environments," in *Proceedings of The 9th Conference on Robot Learning*. PMLR, 2025, pp. 1452–1469.
- [10] C. Dawson, S. Gao, and C. Fan, "Safe Control With Learned Certificates: A Survey of Neural Lyapunov, Barrier, and Contraction Methods for Robotics and Control," *IEEE Transactions on Robotics*, vol. 39, no. 3, pp. 1749–1767, 2023.
- [11] A. Robey, H. Hu, L. Lindemann, H. Zhang, D. V. Dimarogonas, S. Tu, and N. Matni, "Learning Control Barrier Functions from Expert Demonstrations," in *IEEE Conference on Decision and Control*, 2020, pp. 3717–3724.
- [12] S. Liu, C. Liu, and J. Dolan, "Safe Control Under Input Limits with Neural Control Barrier Functions," in *Conference on Robot Learning (CoRL)*, 2022.
- [13] T. Chen, A. Swann, J. Yu, O. Shorinwa, R. Murai, M. Kennedy, and M. Schwager, "A Control Barrier Function for Safe Navigation with Online Gaussian Splatting Maps," in *IEEE International Conference on Robotics and Automation (ICRA)*, 2025, pp. 11 758–11 765.
- [14] O. So, Z. Serlin, M. Mann, J. Gonzales, K. Rutledge, N. Roy, and C. Fan, "How to Train Your Neural Control Barrier Function: Learning Safety Filters for Complex Input-Constrained Systems," in *IEEE International Conference on Robotics and Automation (ICRA)*, 2024, pp. 11 532–11 539.
- [15] J. J. Choi, D. Lee, K. Sreenath, C. J. Tomlin, and S. L. Herbert, "Robust Control Barrier-Value Functions for Safety-Critical Control," in *IEEE Conference on Decision and Control*, 2021, pp. 6814–6821.
- [16] B. Derajic, S. Bernhard, and W. Hönig, "ORN-CBF: Learning Observation-conditioned Residual Neural Control Barrier Functions via Hypernetworks," 2025, arXiv:2509.16614 [cs].
- [17] M. Harms, M. Jacquet, and K. Alexis, "Safe Quadrotor Navigation Using Composite Control Barrier Functions," in *IEEE International Conference on Robotics and Automation (ICRA)*, 2025, pp. 6343–6349.
- [18] A. Safari and J. B. Hoagg, "Time-Varying Soft-Maximum Control Barrier Functions for Safety in an A Priori Unknown Environment," in *American Control Conference (ACC)*, 2024, pp. 3698–3703.
- [19] H. Yu, C. Hirayama, C. Yu, S. Herbert, and S. Gao, "Sequential Neural Barriers for Scalable Dynamic Obstacle Avoidance," in *IEEE/RSJ International Conference on Intelligent Robots and Systems (IROS)*, 2023, pp. 11 241–11 248, iSSN: 2153-0866.
- [20] L. Lindemann and D. V. Dimarogonas, "Control Barrier Functions for Signal Temporal Logic Tasks," *IEEE Control Systems Letters*, vol. 3, no. 1, pp. 96–101, 2019.
- [21] S. Bansal, M. Chen, S. Herbert, and C. J. Tomlin, "Hamilton-Jacobi reachability: A brief overview and recent advances," in *IEEE Conference on Decision and Control*, 2017, pp. 2242–2253.
- [22] T. G. Molnar and A. D. Ames, "Composing Control Barrier Functions for Complex Safety Specifications," *IEEE Control Systems Letters*, vol. 7, pp. 3615–3620, 2023.
- [23] N. Pérez-Higueras, R. Otero, F. Caballero, and L. Merino, "HuNavSim: A ROS 2 Human Navigation Simulator for Benchmarking Human-Aware Robot Navigation," *IEEE Robotics and Automation Letters*, vol. 8, no. 11, pp. 7130–7137, 2023.
- [24] X. Zhang, A. Liniger, and F. Borrelli, "Optimization-Based Collision Avoidance," *IEEE Transactions on Control Systems Technology*, vol. 29, no. 3, pp. 972–983, 2021.
- [25] J. Zeng, B. Zhang, and K. Sreenath, "Safety-Critical Model Predictive Control with Discrete-Time Control Barrier Function," in *American Control Conference (ACC)*, 2021, pp. 3882–3889.
- [26] N. Piccinelli, F. Vesentini, and R. Muradore, "MPC Based Motion Planning For Mobile Robots Using Velocity Obstacle Paradigm," in *European Control Conference (ECC)*, 2023, pp. 1–6.
- [27] J. A. E. Andersson, J. Gillis, G. Horn, J. B. Rawlings, and M. Diehl, "CasADi: a software framework for nonlinear optimization and optimal control," *Mathematical Programming Computation*, vol. 11, no. 1, pp. 1–36, 2019.
- [28] M. Tayal, R. Singh, J. Keshavan, and S. Kolathaya, "Control Barrier Functions in Dynamic UAVs for Kinematic Obstacle Avoidance: A Collision Cone Approach," in *American Control Conference (ACC)*, 2024, pp. 3722–3727, iSSN: 2378-5861.
- [29] W. Xiao and C. Belta, "High-Order Control Barrier Functions," *IEEE Transactions on Automatic Control*, vol. 67, no. 7, pp. 3655–3662, 2022.
- [30] S. Bansal and C. J. Tomlin, "DeepReach: A Deep Learning Approach to High-Dimensional Reachability," in *IEEE International Conference on Robotics and Automation (ICRA)*, 2021, pp. 1817–1824, iSSN: 2577-087X.
- [31] Z. Feng, L. Qiu, and S. Bansal, "Bridging Model Predictive Control and Deep Learning for Scalable Reachability Analysis," in *Proceedings of Robotics: Science and Systems*, vol. 21, 2025.